ACS APPLIED ENERGY MATERIALS
Cite This: ACS Appl. Energy Mater. 2018, 1, 5033−5042
Article
www.acsaem.org

Examining Structure−Property−Function Relationships in Thiophene, Selenophene, and Tellurophene Homopolymers

Joseph G. Manion,[†] Shuyang Ye,[†] Andrew H. Proppe,[†,‡] Arnaud W. Laramée,[†] George R. McKeown,[†] Emily L. Kynaston,[†] Shana O. Kelley,[†,§] Edward H. Sargent,[‡] and Dwight S. Seferos*[,†,∥]

[†]Department of Chemistry, University of Toronto, 80 St. George Street, Toronto, Ontario M5S 3H6, Canada
[‡]Department of Electrical and Computer Engineering, University of Toronto, 10 King's College Road, Toronto, Ontario M5S 3G4, Canada
[§]Leslie Dan Faculty of Pharmacy, Department of Pharmaceutical Sciences, University of Toronto, 144 College Street, Toronto, Ontario M5S 3M2, Canada
[∥]Department of Chemical Engineering and Applied Chemistry, University of Toronto, 200 College Street, Toronto, Ontario M5S 3E5, Canada

Supporting Information

ABSTRACT: Heavy atom main group element-containing conjugated polymers have attracted increasing attention in recent years. The synthesis of these compounds is generally involved, and little is known about their optoelectronic device performance. Here we examine the relationship between polymer structure and optoelectronic behavior in a series of chalcogenophene homopolymers of thiophene, selenophene, and tellurophene with well-matched molecular weights, dispersity, and regioregularity. We employ fast and slow drying device preparations to study the effect of polymer−fullerene separation on charge separation and collection in canonical bulk heterojunction photovoltaic cells. In both preparations, increasing heteroatom size leads to larger proportions of finely mixed polymer−fullerene domains. Differences in polymer−fullerene separation between preparations result in the formation of optimal morphologies in selenophene and tellurophene devices with little impact on thiophene devices. We then use planar heterojunction devices to directly examine the effects of heteroatom substitution on charge transport and charge generation and find that in the absence of polymer−fullerene mixing, devices exhibit similar diode behavior. We further demonstrate that ultrafast decay pathways unique to heavy heteroatom-containing polymers are apparent in both planar and bulk heterojunctions and thus not dependent on polymer−fullerene mixing or polymer assembly. This work directly examines the role of heteroatom substitution in defining the photovoltaic performance of conjugated homopolymers. Through single-atom substitution we are able to significantly modify polymer assembly, mixing, and optoelectronic properties. Specific emphasis on tellurophene polymers reveals relationships between polymer structure and properties that are not apparent in more traditional light-atom chalcogenophenes such as thiophene and selenophene.

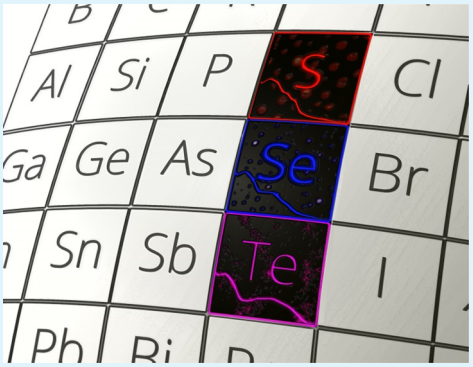

KEYWORDS: *chalcogenophenes, organic photovoltaics, donor−acceptor mixing, heavy atom effects, bulk-heterojunction, planar-heterojunction, ultrafast decay*

INTRODUCTION

Conjugated polymers are of great interest because of their potential as less expensive, lightweight, and flexible alternatives to traditional semiconductors.[1−3] Key to the use of these polymers is a fundamental understanding of their structure−property relationships, which has proven essential to optimizing device performance.[4−7] Heteroatom substitution in conjugated polymers is an approach to control polymer energy levels, optical bandgaps, and solid-state assembly.[8−14] In recent years, several examples of conjugated polymers that contain main group elements such as B, Al, Si, Ge, P, Se, and Te have emerged.[15−22] These polymers allow for studying the effect of single-atom substitution in conjugated polymers and how that influences properties. Yet the majority of these studies have not investigated the optoelectronic device performance of these emerging new compositions, presumably because of challenges associated with larger-scale synthesis and stability.

To effectively study the role of heteroatoms requires controlled polymerization methods to negate the influence of polymer molecular weight, dispersity, and regioregularity. Poly(3-alkylthiophene)s deserve special consideration when one considers the role that conjugated polymers have played in developing structure−property relationships. This is because

Received: June 27, 2018
Accepted: September 4, 2018
Published: September 13, 2018

DOI: 10.1021/acsaem.8b01023
ACS Appl. Energy Mater. 2018, 1, 5033−5042

Table 1. Polymer M_n, Dispersity, Absorption Max and Onset, Monomer Molar Absorption Coefficient (ε), HOMO (CV), and E_g

polymer	M_n (kDa)	$Đ$	λ_{max}^{film} (nm)	λ_{onset}^{film} (nm)	ε (M^{-1} cm^{-1})	HOMO−CV (eV)	E_g (eV)
PTh	41.0	1.2	528	649	8 152	−5.34	1.91
PSe	39.0	1.2	587	751	8 644	−5.28	1.65
PTe	36.6	1.2	676	855	10 549	−5.05	1.45

they are the only type of conjugated polymer that can be prepared in a manner that controls chain length, dispersity, and end group functionality. Heteroatom derivatives of poly(3-alkylthiophene) have served as model systems for studying structure−property relationships in group-16 polymers.[10−12,23−25] Relative to the lighter analogues, poly(3-alkylselenophene)s and poly(3-alkyltellurophene)s (P3ATe) exhibit a narrow optical bandgap, increased planarity and polarizability, and unique photophysical behavior.[26−31]

Until now, tellurophene has been incorporated primarily as a linker or comonomer or in short-chain homopolymers with broad dispersity.[32−42] Homopolymers of P3ATe have received little attention because of their limited solubility and the corresponding synthetic challenges associated with achieving controlled polymerization.[23,32,43−45] In 2016 our group reported a reliable route for producing P3ATe with the same degree of control that was previously observed only for poly(3-alkylthiophene).[45] P3ATes are underexplored relative to many other classes of conjugated polymers.[46] Herein we report the first systematic study of the full series of group 16 polymers (polythiophene, polyselenophene, and polytellurophene) functionalized with large, branched alkyl chains to ensure similar solubility. By comparing these polymers as donor materials in organic photovoltaics (OPVs) processed using identical conditions in different configurations, we highlight the impact of heavier heteroatoms on optoelectronic properties, donor−acceptor separation, and polymer assembly.

RESULTS AND DISCUSSION

Catalyst-transfer polycondensation (CTP) was used to produce well-defined conjugated polymers as described in our previous work.[47−50] In this study, a commercially available 3,7-dimethyloctyl (DMO) alkyl chain was chosen to facilitate synthesis and confer high solubility. All polymers were prepared in similar M_n regimes with approximately equal $Đ$ (Table 1) and high regioregularity (over 96%), as confirmed by gel permeation chromatography (GPC) (Figure S1) and ^{1}H NMR (Figure S2). Regioregularity was measured according to literature procedures by integrating the methylene signals in the ^{1}H NMR spectra (Figure S2a, inset).[51]

Devices and thin films were prepared using fast and slow drying methods to assess heteroatom influence on polymer processing, order, and performance. Slow conditions increase polymer−fullerene separation and demonstrate the influence of isolated donor and acceptor domains on device performance. Fast dried samples highlight the relative ability of each polymer to separate from fullerene using conditions designed to increase the extent of polymer−fullerene mixing. Together the two preparations reflect how heteroatom substitution changes the capacity of the respective polymers to separate from fullerene, transport charge and contribute to the device photocurrent. Fast dried samples were prepared by rapidly spin coating solutions from chlorobenzene, whereas slow dried samples were prepared by slow spin coating from solutions of *o*-dichlorobenzene. Consistent with previous reports, heteroatom substitution results in red-shifted absorbance in both fast and slow dried thin films relative to solutions (Figure 1).[23]

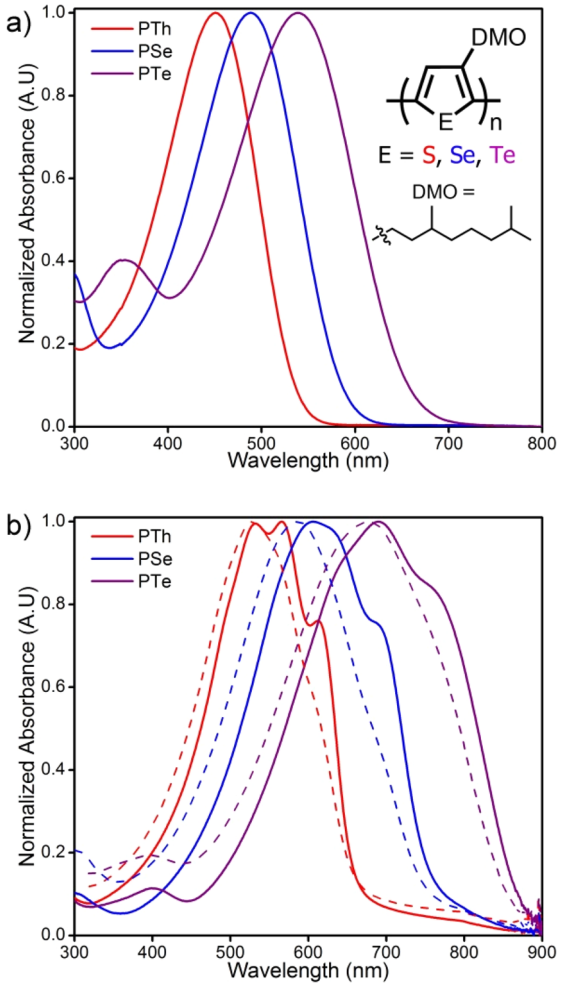

Figure 1. Polymer chemical structures and optical absorption spectra of (a) solutions and (b) fast (dashed) and slow (solid) dried thin films.

In both films, absorption maxima were found to redshift between 60 and 90 nm upon substitution with heavier atoms. PTe samples exhibit significant broadening of the maximum absorption feature because of the lower-energy bandgap. Characteristic of this broadening, the vibronic structure present in all solid-state samples is most evident in PTh and least so in PTe (Figure 1). Optical bandgaps were calculated from the absorption onset in fast dried thin films (Table 1). Highest occupied molecular orbital (HOMO) levels were determined using cyclic voltammetry (CV) (Figure S3) on drop cast films (Table 1) and are consistent with those previously reported.[23] Because of the similar M_n and the high solubility afforded by the identical side chains, we attribute the differences in polymer ordering to the influence of the

DOI: 10.1021/acsaem.8b01023
ACS Appl. Energy Mater. 2018, 1, 5033−5042

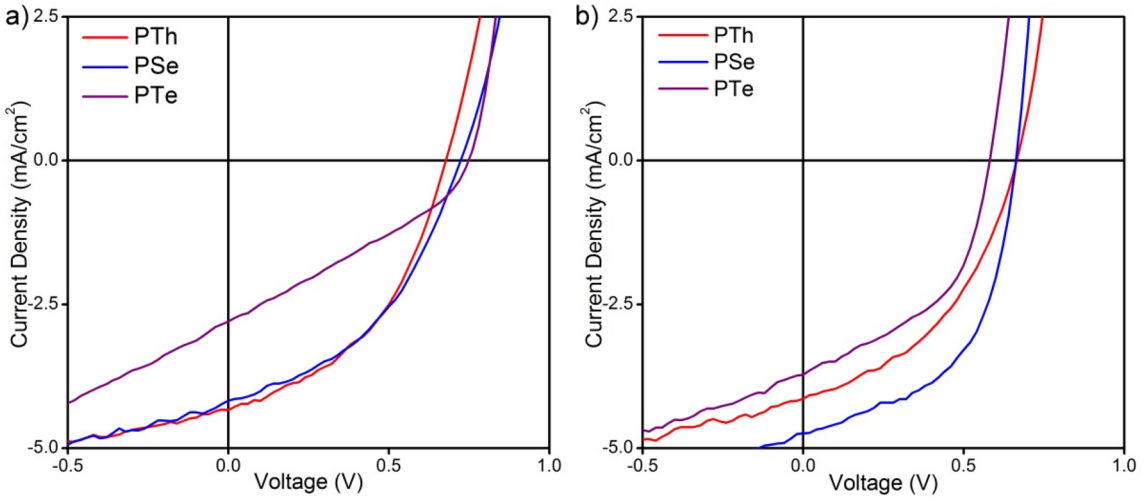

Figure 2. *J*–*V* curves of (a) fast and (b) slow dried devices.

heteroatom and find that it has a significant impact on assembly in both sets of films.[52−54]

Polymer morphology was initially examined in bulk heterojunction devices prepared by blending polymers (PTh/PSe/PTe) with $PC_{71}BM$ in a 1:1.5 ratio in chlorobenzene for fast dried films and in a 1:0.8 ratio in *o*-dichlorobenzene for slow dried conditions. Fast deposition conditions were optimized to ensure reliable formation of high-quality thin films free from visible aggregates. Slow dried devices were vapor annealed through evaporation of residual solvent to examine the ability of the respective polymers to assemble. The stronger vibronic features in slow dried films compared to fast samples reflect increased polymer order (Figure 1b). These conditions significantly altered polymer–fullerene separation leading to substantial differences in performance, most evident in PSe and PTe devices. From the relative intensity of the vibronic features, it is apparent that the degree of $\pi-\pi$ stacking is reduced on substitution with heavier heteroatoms. This observation is consistent with previous reports that demonstrate heavy atoms result in larger disordered domains.[52] This leads to distinct polymer assembly and polymer–fullerene mixing, most pronounced in BHJ devices prepared using PTe.

Despite the significant difference in polymer–fullerene ratios between fast and slow dried devices, the power conversion efficiency (PCE) in PTh devices is similar between samples because of minor variations in short circuit current density (J_{sc}) and fill factor (FF) (Figure 2). In PSe and PTe, differences are more pronounced resulting in average PCE increases of 123% and 155% for the respective slow dried devices (Tables 2 and 3). These improvements result from differences in charge collection and generation that depend heavily on polymer–fullerene assembly and optoelectronic effects of heteroatom substitution. In PSe and PTe devices, the influence of the heteroatom is particularly apparent in the J_{sc}. Differences in J_{sc} depend on several factors, including device absorption, charge separation, and carrier collection. In all fast dried devices, excess $PC_{71}BM$ dominates absorption profiles, whereas slow dried devices show stronger polymer contributions (Figure 3a,c). Secondary ion mass spectrometry of fast dried devices shows that though absorption profiles appear to be primarily due to strong fullerene contributions, the respective polymers are present in the blend films, with clear signals from the respective heteroatoms (Figure S4). Though PTe has the highest molar absorption coefficient (Table 1 and Figure S5), thin films of similar thickness show the lowest absorption for PTe (Figure S6), consistent with slow dried device profiles (Figure 3c). Polymer absorption maxima are blue-shifted in fast dried devices and are similar to their pristine solution spectra, reflecting disruption of polymer order in these blends (Figure 3a). In slow dried devices, the complementary absorption of PSe and PTe relative to $PC_{71}BM$ increases J_{sc} (Table 3). These differences are apparent in the external quantum efficiency (EQE) traces of fast and slow dried devices (Figure 3 b,d). In all fast dried devices, the EQE shows minimal contribution beyond 700 nm, consistent with the blend absorption. Slow dried devices show significant contributions from PSe beyond 700 nm with minor contributions from PTe as far as 800 nm (Figure 3d).

In both fast and slow devices, EQE measurements show that PTe contributes lower photocurrent at its absorption maxima than PTh and PSe. This indicates charge generation and/or collection in PTe devices is less efficient compared to PTh and PSe. This is jointly attributed to heavy-atom specific photophysics and morphology. Previous work has demonstrated that poly(3-alkylselenophenes) and tellurophenes are capable of rapid intersystem crossing to produce triplets.[27−29,34] Consistent with these findings, ultrafast transient absorption experiments and fluorescence spectra show more efficient decay for PSe and PTe with significantly decreased

Table 2. Photovoltaic Performance of Fast Dried Devices

polymer	V_{oc} (V)	J_{sc} (mA cm^{-2})	FF (%)	PCE_{max} (%)	PCE_{avg} (%)[a]
PTh	0.67	4.31	45.0	1.30	1.20 ± 0.06
PSe	0.73	4.16	42.4	1.29	1.25 ± 0.02
PTe	0.75	2.77	31.1	0.64	0.60 ± 0.04

[a]Average PCE of 10 devices ± 1 standard deviation (σ).

Table 3. Photovoltaic Performance of Slow Dried Devices

polymer	V_{oc} (V)	J_{sc} (mA cm^{-2})	FF (%)	PCE_{max} (%)	PCE_{avg} (%)[a]
PTh	0.67	4.11	43.0	1.18	1.10 ± 0.05
PSe	0.67	4.74	51.9	1.65	1.54 ± 0.06
PTe	0.59	3.69	46.9	1.02	0.93 ± 0.07

[a]Average PCE of 10 devices ± 1 standard deviation (σ).

DOI: 10.1021/acsaem.8b01023
ACS Appl. Energy Mater. 2018, 1, 5033−5042

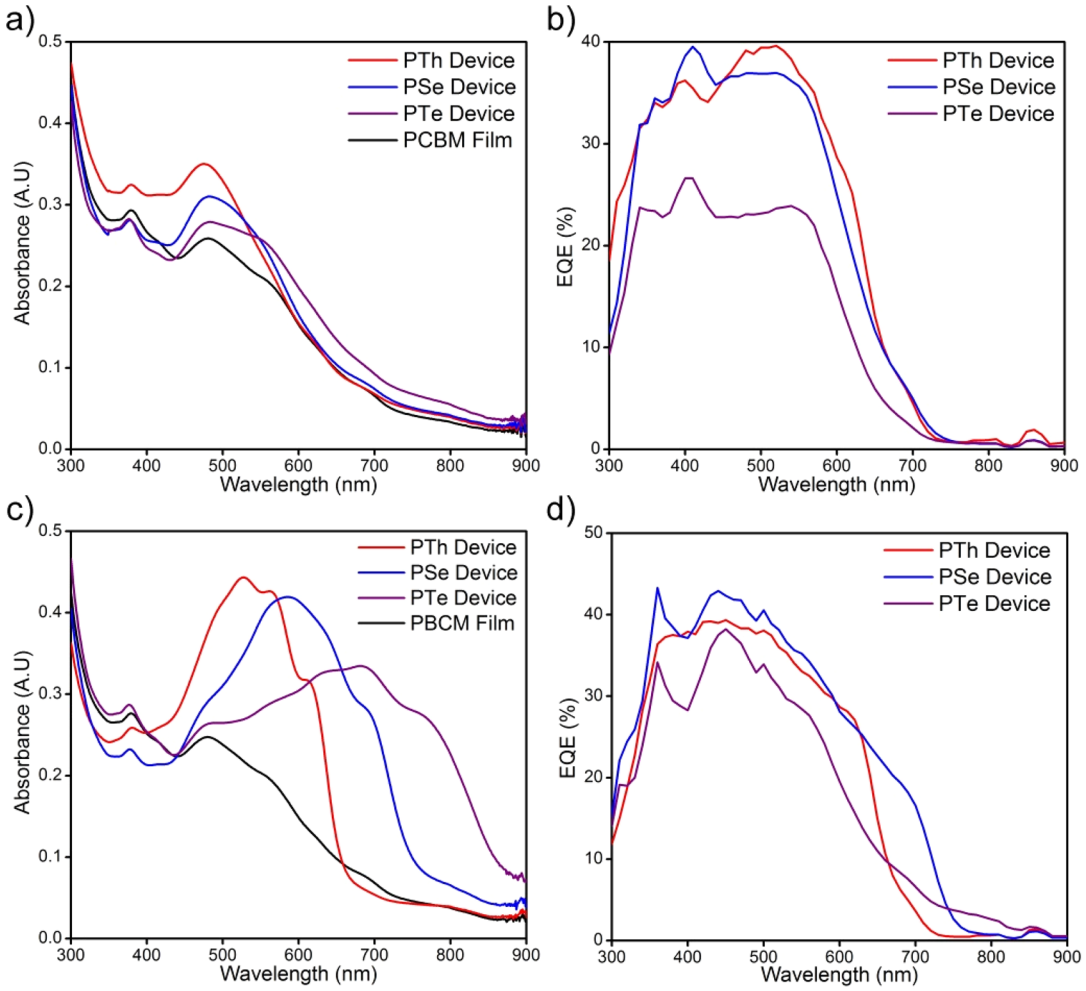

Figure 3. Optical absorption spectra (a and c) and external quantum efficiency (b and d) of fast and slow dried devices.

fluorescence intensity relative to PTh (Figure 4a, b). PTe specifically exhibits no obvious fluorescence and has the largest decrease in amplitude of the bleach signal within the instrument response time, regardless of excitation power (Figure 4). Together these observations suggest that intersystem crossing is more efficient in PTe,[55−57] which may contribute to its weaker contribution in the EQE of both fast and slow dried devices. Recombination losses via triplet states involve kinetic competition between triplet formation, charge separation, and charge extraction.[58−60] In bulk-heterojunction devices, polymer−fullerene separation can influence the competition between charge separation and triplet formation. In PTe-containing devices, intersystem crossing and decreased polymer−fullerene separation increase the potential impact of triplet states relative to lighter analogues.

While current shows strong influence from the optoelectronic effects specific to heavier heteroatoms, polymer−fullerene mixing is responsible for substantial differences in V_{oc} and FF. In fast dried devices, open-circuit voltage (V_{oc}) increases from PTh to PSe to PTe (Figure 2a and Table 2), whereas slow dried devices exhibit a reversed trend (Figure 2b and Table 3). Comparison of fast and slow dried BHJ devices shows minimal variation in the V_{oc} of PTh and PSe devices. PTh devices exhibit similar performance in both configurations with identical V_{oc}, whereas PSe devices show a 60 mV decrease in slow dried devices. The dramatic difference of 160 mV between the two device configurations in PTe reflects the stronger impact of heavier heteroatoms on polymer assembly and mixing with fullerene.

In bulk heterojunction devices, V_{oc} and FF are heavily dependent on the formation of an optimal donor−acceptor morphology. In all slow dried devices, increased polymer order improves separation from fullerene resulting in better charge separation and collection, consistent with increases in J_{sc} and FF. These effects are least evident in PTh, which has the greatest capacity to separate from fullerene regardless of deposition conditions. The effects of donor−acceptor separation are more pronounced in the fast dried devices based on PSe and PTe. In the slow dried BHJ devices, the decrease in V_{oc} from PTh to PSe to PTe is consistent with the CV-derived HOMO levels of the respective polymers, the greater separation of polymer and fullerene afforded by slow-drying, and with the increased order in the polymers evident in the absorption spectra (Figure 1b). In contrast, in fast dried devices, polymer and fullerene separation is limited by the polymer's ability to form ordered domains. In these devices, V_{oc} follows a reverse trend. Increased polymer disorder has been shown to increase V_{oc} because of changes in polymer−fullerene mixing and electronic properties.[52,61,62] Increased intermixing in PTe is consistent with previous reports examining analogues of poly(thiophene) and selenophene.[52]

DOI: 10.1021/acsaem.8b01023
ACS Appl. Energy Mater. 2018, 1, 5033−5042

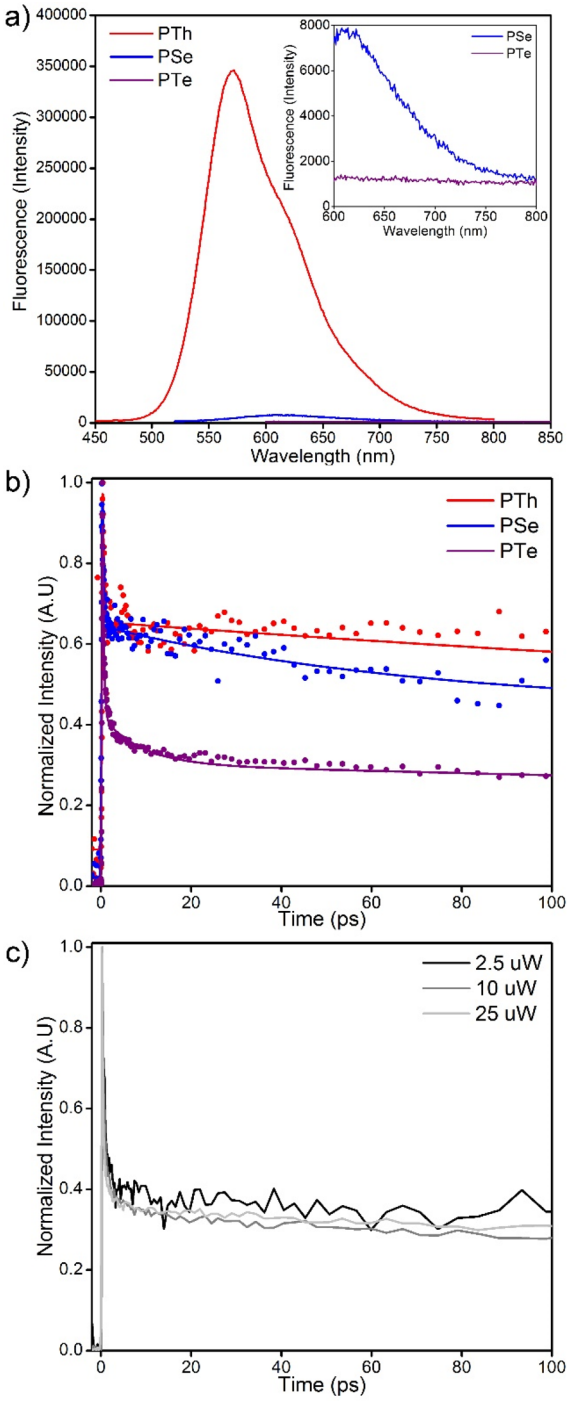

Figure 4. (a) Fluorescence intensity (inset: zoomed in PSe and PTe traces). Excitation wavelengths of 450, 490, and 540 nm were used for PTh, PSe and PTe, respectively. (b) Time traces from ultrafast transient absorption measurements for polymer solutions (dots) with triexponential fitting (lines). Traces are taken from the bleach maximum of the band edge. (c) Power-dependent decay traces of PTe.

We suggest that the increase in V_{oc} in fast dried PSe and PTe devices relative to slow dried devices results from changes in polymer electronics and mixing due to disorder. Wide-angle X-ray scattering plots demonstrate that all polymers exhibit pronounced long-range out-of-plane order in slow dried device films (Figure S7). In these samples the fwhm increases with heavy atom substitution, suggesting smaller and more defective crystalline domains are formed. Consistent with previous reports, we find that heavier atoms decrease out-of-plane *d*-spacing, reflecting increased planarity in PSe and PTe (Table S1).[12] While all samples show ordered domains by WAXS, the decrease in $\pi-\pi$ stacking observed in heavy atom-containing polymers (Figure 1b) suggests a fraction of disordered phase is present. These results agree with previous findings that demonstrate $\pi-\pi$ stacking decreases with heavier atoms and corresponds to a larger disordered fraction.[52,54] While these differences increase V_{oc} relative to slow dried conditions, poor percolation and excessive intermixing between the polymer and fullerene limit FF and J_{sc} modestly in PSe and significantly in PTe. The low FF and abnormal $J-V$ trace of fast dried PTe devices indicate nonoptimal morphology and suggest significant strong resistive effects are present in PTe devices. However, dark $J-V$ traces of the respective devices show little evidence of anomalous diode behavior (Figure S8).

To demonstrate the impact of heteroatom substitution on polymer–fullerene blending we studied devices using a combination of atomic force microscopy (AFM) and transmission electron microscopy (TEM). Both AFM and TEM of fast dried devices demonstrate that donor–acceptor phase separation increases from PTe to PSe to PTh (Figures 5a and S9). The large clusters present in both PTh and PSe devices were identified by kelvin probe force microscopy (KPFM) as $PC_{71}BM$ aggregates, coated with a thin layer of polymer (Figure S10).[63] The presence of large $PC_{71}BM$ domains indicates polymer–fullerene separation, allowing for current collection, resulting in higher J_{sc}, FF, and EQE for PTh and PSe fast dried devices. In PSe devices, the $PC_{71}BM$ aggregates are substantially smaller than in PTh, suggesting that similar to tellurium, selenium limits the growth of $PC_{71}BM$ domains during fast deposition. In stark contrast to the two lighter polymers, fast dried PTe device surfaces (AFM) and bulk (TEM) do not contain $PC_{71}BM$ aggregates, indicating very minor phase separation (Figures 5a and S9–S11a) and fine intermixing. Though the large aggregates of polymer-coated $PC_{71}BM$ observed for PTh are not ideal and can act as recombination sites, the absence of sufficient donor–acceptor phase separation in PTe films limits charge extraction from the bulk and introduces local trap sites, resulting in strong light-induced resistive effects.

Increased order is evident for all polymers in slow dried devices (Figures 5b and S11b), improving carrier collection, transport, and extraction. In PSe and PTe, this is clear from significant improvements in J_{sc}, FF, and PCE. Increased FF in these devices can be attributed to improved charge transport in ordered polymers and optimal polymer–fullerene separation compared to fast dried samples.[4,64,65] Topography, phase, and KPFM images show polymer-coated $PC_{71}BM$ aggregates remain a prominent feature of PTh samples in slow dried devices (Figures 5b, S11b, and S12). These subsurface $PC_{71}BM$ clusters withdraw electrons from the polymer coating at the upper interface, producing hole-enriched polymer skins adjacent to the aluminum cathode which limit electron extraction.[63,66–68] The presence of fullerene aggregates in both fast and slow dried devices reinforces that PTh exhibits similar polymer–fullerene separation regardless of preparation. In contrast, PSe and PTe phase and KPFM images show minimal aggregation of $PC_{71}BM$ with pronounced fiber-like polymer nanostructures. This morphology and nanoscale assembly results in substantial improvements to the overall performance of slow dried PSe and PTe devices through

DOI: 10.1021/acsaem.8b01023
ACS Appl. Energy Mater. 2018, 1, 5033–5042

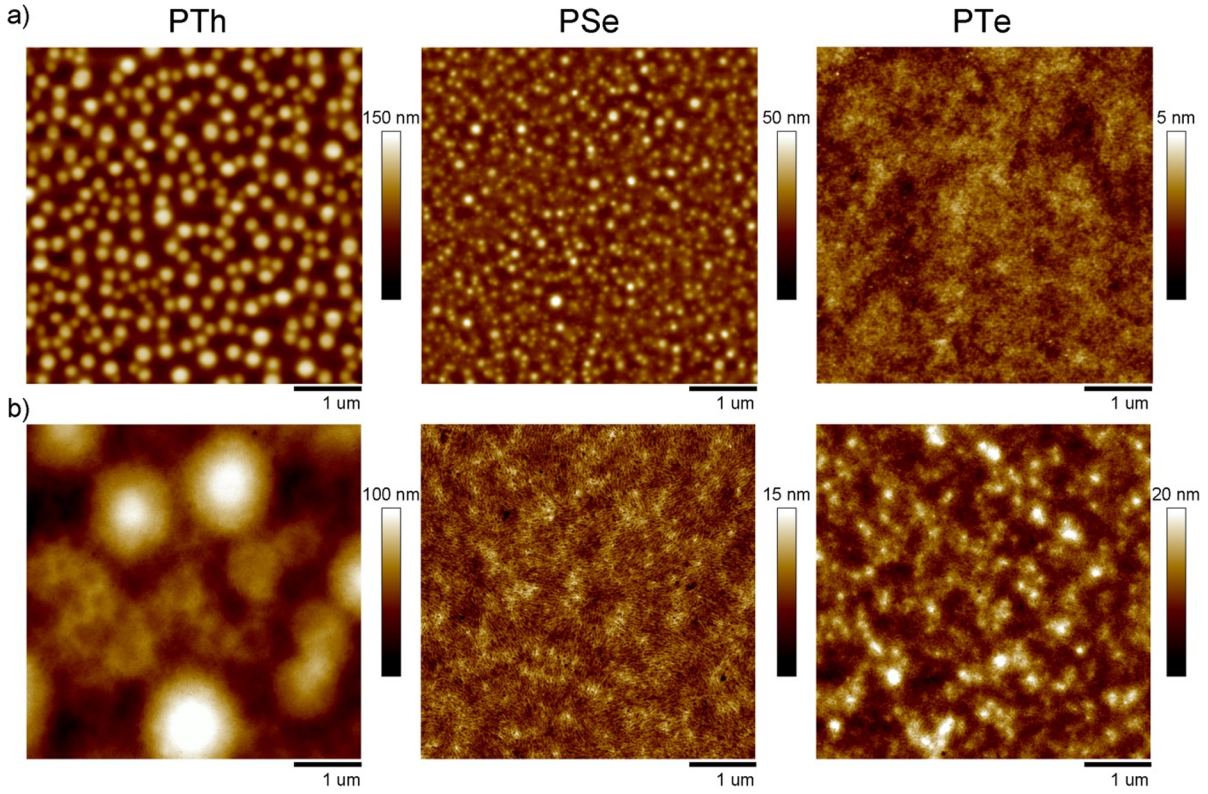

Figure 5. Atomic force microscopy images (tapping mode topography) of (a) fast dried (5 × 5 μm^2) and (b) slow dried (5 × 5 μm^2) devices.

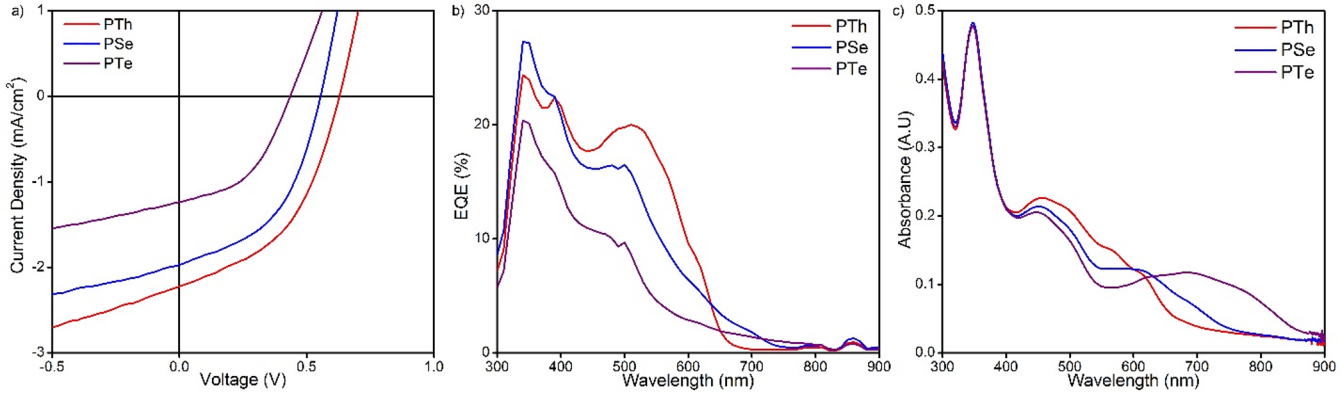

Figure 6. (a) J–V curves, (b) external quantum efficiency, and (c) absorption profiles of planar heterojunction devices.

complementary absorption with fullerene and improved charge collection.

To further examine the impact of these heteroatom substitutions, planar heterojunction devices (PHJs) were prepared using thin layers of polymer (~15 nm) and C_{60} (30 nm). These devices highlight the impact of polymer properties in the absence of the complex polymer–fullerene mixing found in BHJs. In PHJ devices, PTe exhibits the lowest J_{sc} and shows minimal contribution to the EQE at peak polymer absorption (~700 nm) (Figure 6), with the majority of current contribution derived from C_{60} (Table 4). As observed in BHJ devices, polymer contribution to EQE in PHJs is considerably lower for PSe and PTe. Despite the similar thickness, absorption intensity, and identical device design of the PHJ cells, it is clear that heteroatom substitution impacts performance independent of blend morphology and that this effect becomes more prominent as heavier heteroatoms are introduced.

Table 4. Photovoltaic Performance of Planar Heterojunction Devices

polymer	V_{oc} (V)	J_{sc} (mA cm^{-2})	FF (%)	PCE_{max} (%)	PCE_{avg} (%)[a]
PTh	0.63	2.21	46.0	0.64	0.60 ± 0.02
PSe	0.55	1.96	48.2	0.52	0.50 ± 0.01
PTe	0.43	1.23	47.3	0.25	0.23 ± 0.01

[a]Average PCE of 10 devices ± 1 standard deviation (σ).

In PHJs, the trends in V_{oc} and FF are similar to slow dried devices. As planar devices do not involve complex mixing, these devices directly reflect the polymer properties and suggest efficient and balanced transport is maintained with heteroatom substitution. Together, PHJ and BHJ devices help establish the role of heteroatom substitution in modifying

DOI: 10.1021/acsaem.8b01023
ACS Appl. Energy Mater. 2018, 1, 5033–5042

optoelectronic behavior and polymer−fullerene assembly. Further examination of this series of polymers will improve rational design of optimal polymer−fullerene separation to simultaneously maximize V_{oc}, J_{sc}, and FF and will serve as a model system for studying the role of ultrafast decay pathways in organic photovoltaics.

CONCLUSIONS

We have performed the first systematic study of the full series of group 16 polymers in organic photovoltaic devices. Poly(3-alkylthiophene), selenophene, and tellurophene were prepared with similar molecular weight, narrow dispersity, and high regioregularity using controlled polymerization. The effects of heteroatom substitution were examined in bulk and planar heterojunction organic photovoltaics. Two device preparation procedures (fast and slow dried) were used to prepare different bulk heterojunctions from each polymer. The increased mixing of heavy atom-containing PSe and PTe polymers with fullerene results in drastic differences in performance between fast and slow dried bulk heterojunctions when compared to PTh, which is relatively insensitive to drying procedures. Planar heterojunction devices were used to negate the impact of polymer−fullerene mixing and highlight the specific optoelectronic properties resulting from heteroatom substitution. From these devices we observe a reduced contribution to photocurrent that is more apparent with increasing atomic number. On the other hand, heavy atom-containing polymers show improved charge transport and collection when polymers are given the opportunity to order and separate from fullerene in slow dried BHJs and in PHJ devices where polymer−fullerene blending does not impact performance. Despite its lower performance, PTe best demonstrates the potential impacts of heteroatom substitution on polymer−fullerene assembly, optoelectronic properties, and photovoltaic activity. Specifically, a greater capacity for rapid intersystem crossing and polymer−fullerene intermixing are the highest in PTe. We believe that further optimization of P3ATes will enable evaluating the role of triplets in organic electronics and in improving the operating voltage of OPVs by controlling polymer order and mixing with fullerene. By further developing an understanding of the effect of heavy atom substitution on polymer order, we intend to exploit its potential for improving optoelectronic devices.

EXPERIMENTAL SECTION

Materials. PTh, PSe, and PTe were synthesized according to previous literature reports as described below. Chlorobenzene, chloroform, *o*-dichlorobenzene, acetonitrile, tetrabutylammonium hexafluorophosphate, and ferrocene were purchased from Sigma-Aldrich. $PC_{71}BM$ (ADS71BFA) and C_{60} (ADS60BFA) were purchased from American Dye Source. Spectrograde chloroform was purchased from ACP Chemicals. PEDOT:PSS (Clevios P VP AI 4083) was purchased from Heraeus. All materials were used as received unless otherwise indicated.

Monomer Synthesis and General Polymer Preparation. Thiophene, selenophene, and tellurophene monomers were functionalized at the three position with 3,7-dimethyloctyl chains according to previous literature.[45] Polymerizations were carried out by adding isopropylmagnesium chloride (0.98 equiv) to dihalogenated side-chain functionalized monomer in THF followed by stirring for 15 min at room temperature before transferring to a Schlenk flask containing the Ni(dppe)Cl_2 catalyst. A catalyst loading of (150:1 monomer:-catalyst) was used for all polymers. The complete mixture was stirred at room temperature for thiophene and selenophene and at 40 °C for tellurophene for 1 h, followed by quenching in dilute HCl, precipitation in methanol, and purification through sequential Soxhlet extractions in methanol, hexanes, and chloroform. Chloroform fractions were concentrated under vacuum, yielding the final polymer. PTh, PSe, and PTe were collected from chloroform fractions with yields of 49%, 52%, and 55%, respectively. Column chromatography of polymers in chloroform was used to further purify samples prior to examination.

Device Fabrication. ITO-coated glass substrates (Thin Film Devices inc) were cleaned by ultrasonication in aqueous detergent, deionized water, acetone, and methanol followed by treatment in an oxygen plasma-cleaner. PEDOT:PSS was filtered through 0.45 μm PVDF syringe filters and was spin coated at 3000 rpm, followed by annealing at 135 °C for 15 min in ambient. PEDOT-coated ITO was transferred to a nitrogen-filled glovebox at <5 ppm of O_2. Planar heterojunctions were prepared by dissolving group 16 polymers (PTh, PSe, and PTe) in chlorobenzene at 5 mg mL^{-1}. Fast dried samples were prepared by dissolving group 16 polymers in chlorobenzene at 10 mg mL^{-1}. Device blends were mixed with $PC_{71}BM$ in a 1:1.5 ratio (Polymer:$PC_{71}BM$). Slow dried samples were prepared by dissolving group 16 polymers in *o*-dichlorobenzene at 15 mg mL^{-1} for films followed by mixing with $PC_{71}BM$ in a 1:0.8 ratio (Polymer:$PC_{71}BM$) for devices. Fast dried device solutions were stirred for 3 h at 60 °C prior to casting. Slow dried device solutions were stirred for 3 h at 80 °C prior to casting. All solutions were passed through 0.45 μm PTFE syringe filters immediately prior to spin-casting and were cast at 2000 rpm for 30 s for planar and fast dried devices and 800 rpm for 30 s for slow dried devices. Bulk heterojunction photovoltaic devices were completed by deposition of LiF (1 nm) and Al (100 nm). Planar heterojunction devices were completed by deposition of C_{60} (30 nm) followed by deposition of Al (100 nm). C_{60} was deposited using an Angstrom Engineering (Kitchener, Ontario) Nexdep at 10^{-7} Torr. All contacts were deposited by thermal evaporation using an Angstrom Engineering (Kitchener, Ontario) Covap II at 10^{-6} Torr. Device area was defined by shadow masking (0.07 cm^2).

Sample Preparation. Polymer and blend films for optical absorption spectroscopy were prepared on glass slides cleaned by ultrasonication in aqueous detergent, deionized water, acetone, and methanol. Fast and slow dried samples for polymer-only films and device blends were prepared as above on bare glass substrates. Thin-film polymer samples with similar thickness for absorption spectroscopy were prepared as described for fast polymer-only samples using 20 mg mL^{-1} solutions to increase thickness. Layer thicknesses were measured over five points per film using an atomic force microscope. Solution samples for absorption coefficients were initially prepared at 0.3 mg mL^{-1} in spectrograde chloroform and were diluted to produce five samples with optical densities between 0.2−0.8 per polymer. Three stocks were independently prepared for each polymer. Solution samples for optical absorption spectroscopy and fluorescence spectroscopy were initially prepared at 0.1 mg mL^{-1} in spectrograde chloroform and were diluted to achieve an approximate optical density of 0.1 to minimize reabsorption effects. Polymer films for cyclic voltammetry measurements were drop cast from 10 mg mL^{-1} solutions in $CHCl_3$ on gold button electrodes. Solution samples for ultrafast spectroscopy were similarly prepared with dilution to an approximate optical density of 0.2 at the first exciton peak in a 2 mm path length cuvette.

Instrumentation. Atomic force microscopy measurements were performed using a Bruker Dimension Icon microscope. Optical absorption spectra were collected using a Varian Cary 5000 spectrometer. Fluorescence spectra were recorded with a Photon Technology International (PTI) QuantaMaster 40-F NA spectrofluorometer equipped with a photomultiplier detector and a xenon arc lamp. Electrochemical measurements were recorded on films in $MeCN/NBu_4PF_6$ (0.1 M) versus Ag/AgCl (scan rate, 100 mV s^{-1}) with Fc/Fc^+ as an internal standard using a BASi Epsilon potentiostat. *J*−*V* curves were collected using a Keithley 2400 source meter under dark and simulated AM 1.5G conditions at a power intensity of 100 mW cm^{-2}. Spectral mismatch was calibrated using a Si-diode with a KG-5 filter. External quantum efficiency was measured using a 300 W Xe arc lamp with an Oriel Cornerstone 260 1/4 m monochromator and were compared with a Si reference cell traceable to the National

DOI: 10.1021/acsaem.8b01023
ACS Appl. Energy Mater. 2018, 1, 5033−5042

Institute of Standards and Technology. Time of flight secondary ion mass spectrometry (ToF-SIMS) was carried out with a ToF-SIMS V instrument (ION-TOF GmbH, Munster, Germany). Spectra were obtained in high-current, high-resolution mode using a 30 keV Bi^+ primary ion beam for analysis of a 500 μm × 500 μm area. Primary ion dose density was limited to 5×10^{11} ions/cm^2. Nuclear magnetic resonance (NMR) spectra were recorded on a Varian Mercury 400 spectrometer (400 MHz). A Viscotek HT-SEC module 350A (140 °C, butylated hydroxytoluene stabilized 1,2,4-trichlorobenzene) was used to determine polymer molecular weights relative to narrow weight distribution polystyrene standards at 485 nm absorbance. Ultrafast measurements were conducted by generating femtosecond laser pulses with a wavelength of 1030 nm at a 5 kHz repetition rate using a regeneratively amplified Yb:KGW laser (PHAROS from Light Conversion). A beam splitter was used to separate the beam into two components, one which pumps an optical parametric amplifier (ORPHEUS, Light Conversion) for ultrafast pump pulses, while the other part was focused into a sapphire or calcium fluoride (CaF_2) crystal for white-light supercontinuum generation to make the probe pulse (350−950 nm window for CaF_2 to probe the PTh samples and a ∼450−950 nm window to probe the PSe and PTe samples). Both pulses were directed into a commercial transient absorption spectrometer (Helios, Ultrafast). Delaying the probe pulse relative to the pump provides a time window of up to 8 ns. The time resolution of these experiments was ∼300 fs, limited by the pump pulse duration. Measurements were performed using pump powers of 2.5, 10, and 25 μW at 530 nm (for PTe), 480 nm (for PSe), and 420 nm (for PTh). The pump spot size was kept to ∼0.40 μm^2 for all wavelengths and powers. Wide-angle X-ray diffraction experiments were performed on slow dried films prepared as indicated above using a Bruker D8 Discover with a DAVINCI.DESIGN diffractometer with a cobalt sealed tube source and a Vantec 500 area detector for data collection. WAXS plots were collected using still frame scans with one frame, a frame exposure of 600 s, and a detector distance of 20 cm.

■ ASSOCIATED CONTENT

Supporting Information

The Supporting Information is available free of charge on the ACS Publications website at DOI: 10.1021/acsaem.8b01023.

Gel permeation chromatography and ^{1}H NMR profiles of polymer samples; cyclic voltammetry traces of polymer samples; secondary ion mass spectrometry of fast dried BHJ devices; absorption coefficients; thin-film ultraviolet visible absorption profiles; WAXS plots; dark $J-V$ characteristics of fast dried BHJ devices; transmission electron microscopy images of fast dried devices; peak force kelvin probe force microscopy and tapping mode phase imaging of fast and slow dried BHJ devices (PDF)

■ AUTHOR INFORMATION

Corresponding Author

*E-mail: dseferos@chem.utoronto.ca.

ORCID

Shana O. Kelley: 0000-0003-3360-5359

Edward H. Sargent: 0000-0003-0396-6495

Dwight S. Seferos: 0000-0001-8742-8058

Notes

The authors declare no competing financial interest.

■ ACKNOWLEDGMENTS

This work was supported by the NSERC of Canada, the Canadian Foundation for Innovation, and the Ontario Research Fund. J.G.M. is grateful for an Ontario Graduate Scholarship and an NSERC Canadian Graduate Scholarship. The authors thank Dr. Peter M. Brodersen of the Ontario Centre for the Characterization of Advanced Materials and Dr Jim Britten and Victoria Jarvis of the McMaster Analytical X-ray Diffraction Facility.

■ REFERENCES

(1) Sirringhaus, H. 25th Anniversary Article: Organic Field-Effect Transistors: The Path Beyond Amorphous Silicon. *Adv. Mater.* **2014**, *26*, 1319−1335.

(2) Nielsen, C. B.; Holliday, S.; Chen, H.; Cryer, S. J.; McCulloch, I. Non-Fullerene Electron Acceptors for Use in Organic Solar Cells. *Acc. Chem. Res.* **2015**, *48*, 2803−2812.

(3) Krebs, F. C.; Espinosa, N.; Hösel, M.; Søndergaard, R. R.; Jørgensen, M. 25th Anniversary Article: Rise to Power - OPV-Based Solar Parks. *Adv. Mater.* **2014**, *26*, 29−39.

(4) Dou, L.; You, J.; Hong, Z.; Xu, Z.; Li, G.; Street, R. A.; Yang, Y. 25th Anniversary Article: A Decade of Organic/Polymeric Photovoltaic Research. *Adv. Mater.* **2013**, *25*, 6642−6671.

(5) Ndjawa, G. O. N.; Graham, K. R.; Mollinger, S.; Wu, D. M.; Hanifi, D.; Prasanna, R.; Rose, B. D.; Dey, S.; Yu, L.; Brédas, J.-L.; McGehee, M. D.; Salleo, A.; Amassian, A. Open-Circuit Voltage in Organic Solar Cells: The Impacts of Donor Semicrystallinity and Coexistence of Multiple Interfacial Charge-Transfer Bands. *Adv. Energy Mater.* **2017**, *7*, 1601995.

(6) Noriega, R.; Rivnay, J.; Vandewal, K.; Koch, F. P. V.; Stingelin, N.; Smith, P.; Toney, M. F.; Salleo, A. A General Relationship between Disorder, Aggregation and Charge Transport in Conjugated Polymers. *Nat. Mater.* **2013**, *12*, 1038−1044.

(7) Hu, Z.; Shao, B.; Geberth, G. T.; Vanden Bout, D. Effects of Molecular Architecture on Morphology and Photophysics in Conjugated Polymers: From Single Molecules to Bulk. *Chem. Sci.* **2018**, *9*, 1101−1111.

(8) Cao, J.; Chen, S.; Qi, Z.; Xiao, Z.; Wang, J.; Ding, L. An Efficient Selenophene-Containing Conjugated Copolymer for Organic Solar Cells. *RSC Adv.* **2014**, *4*, 5085.

(9) Cao, F.-Y.; Tseng, C.-C.; Lin, F.-Y.; Chen, Y.; Yan, H.; Cheng, Y.-J. Selenophene-Incorporated Quaterchalcogenophene-Based Donor−Acceptor Copolymers To Achieve Efficient Solar Cells with J. Sc Exceeding 20 mA/cm 2. *Chem. Mater.* **2017**, *29*, 10045−10052.

(10) Gibson, G. L.; McCormick, T. M.; Seferos, D. S. Atomistic Band Gap Engineering in Donor−Acceptor Polymers. *J. Am. Chem. Soc.* **2012**, *134*, 539−547.

(11) Jeffries-EL, M.; Kobilka, B. M. M.; Hale, B. J. J. Optimizing the Performance of Conjugated Polymers in Organic Photovoltaic Cells by Traversing Group 16. *Macromolecules* **2014**, *47*, 7253−7271.

(12) Carrera, E. I.; Seferos, D. S. Semiconducting Polymers Containing Tellurium: Perspectives Toward Obtaining High-Performance Materials. *Macromolecules* **2015**, *48*, 297−308.

(13) Fei, Z.; Han, Y.; Gann, E.; Hodsden, T.; Chesman, A. S. R.; McNeill, C. R.; Anthopoulos, T. D.; Heeney, M. Alkylated Selenophene-Based Ladder-Type Monomers via a Facile Route for High-Performance Thin-Film Transistor Applications. *J. Am. Chem. Soc.* **2017**, *139*, 8552−8561.

(14) An, Y.; Oh, J.; Chen, S.; Lee, B.; Lee, S. M.; Han, D.; Yang, C. Effects of Incorporating Different Chalcogenophene Comonomers into Random Acceptor Terpolymers on the Morphology and Performance of All-Polymer Solar Cells. *Polym. Chem.* **2018**, *9*, 593−602.

(15) Tsai, C. H.; Fortney, A.; Qiu, Y.; Gil, R. R.; Yaron, D.; Kowalewski, T.; Noonan, K. J. T. Conjugated Polymers with Repeated Sequences of Group 16 Heterocycles Synthesized through Catalyst-Transfer Polycondensation. *J. Am. Chem. Soc.* **2016**, *138*, 6798−6804.

(16) Stolar, M.; Reus, C.; Baumgartner, T. Xylene-Bridged Phosphaviologen Oligomers and Polymers as High-Performance Electrode-Modifiers for Li-Ion Batteries. *Adv. Energy Mater.* **2016**, *6*, 1600944.

DOI: 10.1021/acsaem.8b01023
ACS Appl. Energy Mater. 2018, 1, 5033−5042

(17) Adachi, Y.; Ooyama, Y.; Ren, Y.; Yin, X.; Jäkle, F.; Ohshita, J. Hybrid Conjugated Polymers with Alternating Dithienosilole or Dithienogermole and Tricoordinate Boron Units. *Polym. Chem.* **2018**, *9*, 291−299.
(18) Meng, B.; Ren, Y.; Liu, J.; Jäkle, F.; Wang, L. P-π Conjugated Polymers Based on Stable Triarylborane with N-Type Behavior in Optoelectronic Devices. *Angew. Chem., Int. Ed.* **2018**, *57*, 2183−2187.
(19) Gibson, G. L.; Gao, D.; Jahnke, A. A.; Sun, J.; Tilley, A. J.; Seferos, D. S. Molecular Weight and End Capping Effects on the Optoelectronic Properties of Structurally Related "heavy Atom" Donor−acceptor Polymers. *J. Mater. Chem. A* **2014**, *2*, 14468−14480.
(20) Ding, Z.; Long, X.; Dou, C.; Liu, J.; Wang, L. A Polymer Acceptor with an Optimal LUMO Energy Level for All-Polymer Solar Cells. *Chem. Sci.* **2016**, *7*, 6197−6202.
(21) Dou, C.; Ding, Z.; Zhang, Z.; Xie, Z.; Liu, J.; Wang, L. Developing Conjugated Polymers with High Electron Affinity by Replacing a C□C Unit with a B ← N Unit. *Angew. Chem., Int. Ed.* **2015**, *54*, 3648−3652.
(22) Ji, L.; Griesbeck, S.; Marder, T. B. Recent Developments in and Perspectives on Three-Coordinate Boron Materials: A Bright Future. *Chem. Sci.* **2017**, *8*, 846−863.
(23) Al-Hashimi, M.; Han, Y.; Smith, J.; Bazzi, H. S.; Alqaradawi, S. Y. A.; Watkins, S. E.; Anthopoulos, T. D.; Heeney, M. Influence of the Heteroatom on the Optoelectronic Properties and Transistor Performance of Soluble Thiophene-, Selenophene- and Tellurophene−vinylene Copolymers. *Chem. Sci.* **2016**, *7*, 1093−1099.
(24) Zade, S. S.; Zamoshchik, N.; Bendikov, M. Oligo- and Polyselenophenes: A Theoretical Study. *Chem. - Eur. J.* **2009**, *15*, 8613−8624.
(25) Dang, M. T.; Hirsch, L.; Wantz, G. P3HT:PCBM, Best Seller in Polymer Photovoltaic Research. *Adv. Mater.* **2011**, *23*, 3597−3602.
(26) Jahnke, A. A.; Djukic, B.; McCormick, T. M.; Buchaca Domingo, E.; Hellmann, C.; Lee, Y.; Seferos, D. S. Poly(3-Alkyltellurophene)s Are Solution-Processable Polyheterocycles. *J. Am. Chem. Soc.* **2013**, *135*, 951−954.
(27) Pensack, R. D.; Song, Y.; McCormick, T. M.; Jahnke, A. A.; Hollinger, J.; Seferos, D. S.; Scholes, G. D. Evidence for the Rapid Conversion of Primary Photoexcitations to Triplet States in Seleno- and Telluro- Analogues of Poly(3-Hexylthiophene). *J. Phys. Chem. B* **2014**, *118*, 2589−2597.
(28) Mahrok, A. K.; Carrera, E. I.; Tilley, A. J.; Ye, S.; Seferos, D. S. Synthesis and Photophysical Properties of Platinum-Acetylide Copolymers with Thiophene, Selenophene and Tellurophene. *Chem. Commun.* **2015**, *51*, 5475−5478.
(29) Datko, B. D.; Thomas, A. K.; Fei, Z.; Heeney, M.; Grey, J. K. Effect of a Heavy Heteroatom on Triplet Formation and Interactions in Single Conjugated Polymer Molecules and Aggregates. *Phys. Chem. Chem. Phys.* **2017**, *19*, 28239−28248.
(30) Heeney, M.; Zhang, W.; Crouch, D. J.; Chabinyc, M. L.; Gordeyev, S.; Hamilton, R.; Higgins, S. J.; McCulloch, I.; Skabara, P. J.; Sparrowe, D.; Tierney, S. Regioregular poly(3-Hexyl)selenophene: A Low Band Gap Organic Hole Transporting Polymer. *Chem. Commun.* **2007**, 5061−5063.
(31) Ballantyne, A. M.; Chen, L.; Nelson, J.; Bradley, D. D. C.; Astuti, Y.; Maurano, A.; Shuttle, C. G.; Durrant, J. R.; Heeney, M.; Duffy, W.; McCulloch, I. Studies of Highly Regioregular Poly(3-Hexylselenophene) for Photovoltaic Applications. *Adv. Mater.* **2007**, *19*, 4544−4547.
(32) Park, Y. S.; Kale, T. S.; Nam, C.-Y.; Choi, D.; Grubbs, R. B. Effects of Heteroatom Substitution in Conjugated Heterocyclic Compounds on Photovoltaic Performance: From Sulfur to Tellurium. *Chem. Commun.* **2014**, *50*, 7964−7967.
(33) Park, Y. S.; Wu, Q.; Nam, C. Y.; Grubbs, R. B. Polymerization of Tellurophene Derivatives by Microwave-Assisted Palladium-Catalyzed Ipso-Arylative Polymerization. *Angew. Chem., Int. Ed.* **2014**, *53*, 10691−10695.
(34) Yang, L.; Gu, W.; Lv, L.; Chen, Y.; Yang, Y.; Ye, P.; Wu, J.; Hong, L.; Peng, A.; Huang, H. Triplet Tellurophene-Based Acceptors for Organic Solar Cells. *Angew. Chem., Int. Ed.* **2018**, *57*, 1096−1102.
(35) Duhović, S.; Dincă, M. Synthesis and Electrical Properties of Covalent Organic Frameworks with Heavy Chalcogens. *Chem. Mater.* **2015**, *27*, 5487−5490.
(36) Kaur, M.; Lee, D. H.; Yang, D. S.; Um, H. A.; Cho, M. J.; Kang, J. S.; Choi, D. H. Diketopyrrolopyrrole-Bitellurophene Containing a Conjugated Polymer and Its High Performance Thin-Film Transistor Sensor for Bromine Detection. *Chem. Commun.* **2014**, *50*, 14394−14396.
(37) Li, P. F.; Schon, T. B.; Seferos, D. S. Thiophene, Selenophene, and Tellurophene-Based Three-Dimensional Organic Frameworks. *Angew. Chem., Int. Ed.* **2015**, *54*, 9361−9366.
(38) Lv, L.; Wang, X. X.; Wang, X. X.; Yang, L.; Dong, T.; Yang, Z.; Huang, H. Tellurophene-Based N-Type Copolymers for Photovoltaic Applications. *ACS Appl. Mater. Interfaces* **2016**, *8*, 34620−34629.
(39) Ashraf, R. S.; Meager, I.; Nikolka, M.; Kirkus, M.; Planells, M.; Schroeder, B. C.; Holliday, S.; Hurhangee, M.; Nielsen, C. B.; Sirringhaus, H.; McCulloch, I. Chalcogenophene Comonomer Comparison in Small Band Gap Diketopyrrolopyrrole-Based Conjugated Polymers for High-Performing Field-Effect Transistors and Organic Solar Cells. *J. Am. Chem. Soc.* **2015**, *137*, 1314−1321.
(40) Rivard, E. Tellurophenes and Their Emergence as Building Blocks for Polymeric and Light-Emitting Materials. *Chem. Lett.* **2015**, *44*, 730−736.
(41) Parke, S. M.; Boone, M. P.; Rivard, E. Marriage of Heavy Main Group Elements with π-Conjugated Materials for Optoelectronic Applications. *Chem. Commun.* **2016**, *52*, 9485−9505.
(42) Kobilka, B. M.; Hale, B. J.; Ewan, M. D.; Dubrovskiy, A. V.; Nelson, T. L.; Duzhko, V.; Jeffries-EL, M. Influence of Heteroatoms on Photovoltaic Performance of Donor−acceptor Copolymers Based on 2,6-Di(thiophen-2-yl)benzo[1,2-b:4,5-B′]difurans and Diketopyrrolopyrrole. *Polym. Chem.* **2013**, *4*, 5329.
(43) Lee, W.-H.; Lee, S. K.; Shin, W. S.; Moon, S.-J.; Kang, I.-N. Synthesis and Characterization of Regioregular Poly (3- Dodecyltellurophene). *J. Polym. Sci., Part A: Polym. Chem.* **2013**, *51*, 2753−2758.
(44) Jahnke, A. A.; Seferos, D. S. Polytellurophenes. *Macromol. Rapid Commun.* **2011**, *32*, 943−951.
(45) Ye, S.; Steube, M.; Carrera, E. I.; Seferos, D. S. What Limits the Molecular Weight and Controlled Synthesis of Poly(3-Alkyltellurophene)s? *Macromolecules* **2016**, *49*, 1704−1711.
(46) Jahnke, A. A.; Yu, L.; Coombs, N.; Scaccabarozzi, A. D.; Tilley, A. J.; DiCarmine, P. M.; Amassian, A.; Stingelin, N.; Seferos, D. S. Polytellurophenes Provide Imaging Contrast towards Unravelling the Structure−property−function Relationships in Semiconductor:insulator Polymer Blends. *J. Mater. Chem. C* **2015**, *3*, 3767−3773.
(47) Yokozawa, T.; Ohta, Y. Transformation of Step-Growth Polymerization into Living Chain-Growth Polymerization. *Chem. Rev.* **2016**, *116*, 1950−1958.
(48) Yokoyama, A.; Miyakoshi, R.; Yokozawa, T. Chain-Growth Polymerization for Poly(3-Hexylthiophene) with a Defined Molecular Weight and a Low Polydispersity. *Macromolecules* **2004**, *37*, 1169−1171.
(49) Sheina, E. E.; Liu, J.; Iovu, M. C.; Laird, D. W.; McCullough, R. D. Chain Growth Mechanism for Regioregular Nickel-Initiated Cross-Coupling Polymerizations. *Macromolecules* **2004**, *37*, 3526−3528.
(50) Marrocchi, A.; Facchetti, A.; Lanari, D.; Santoro, S.; Vaccaro, L. Click-Chemistry Approaches to π-Conjugated Polymers for Organic Electronics Applications. *Chem. Sci.* **2016**, *7*, 6298−6308.
(51) Fei, Z.; Boufflet, P.; Wood, S.; Wade, J.; Moriarty, J.; Gann, E.; Ratcliff, E. L.; McNeill, C. R.; Sirringhaus, H.; Kim, J.-S.; Heeney, M. Influence of Backbone Fluorination in Regioregular Poly(3-Alkyl-4-Fluoro)thiophenes. *J. Am. Chem. Soc.* **2015**, *137*, 6866−6879.
(52) Tsoi, W. C.; James, D. T.; Domingo, E. B.; Kim, J. S.; Al-Hashimi, M.; Murphy, C. E.; Stingelin, N.; Heeney, M.; Kim, J.-S. Effects of a Heavy Atom on Molecular Order and Morphology in Conjugated Polymer:Fullerene Photovoltaic Blend Thin Films and Devices. *ACS Nano* **2012**, *6*, 9646−9656.
(53) Kynaston, E. L.; Fang, Y.; Manion, J. G.; Obhi, N. K.; Howe, J. Y.; Perepichka, D. F.; Seferos, D. S. Patchy Nanofibers from the Thin

DOI: 10.1021/acsaem.8b01023
ACS Appl. Energy Mater. 2018, 1, 5033−5042

Film Self-Assembly of a Conjugated Diblock Copolymer. *Angew. Chem., Int. Ed.* **2017**, *56*, 6152−6156.
(54) Razzell-Hollis, J.; Fleischli, F.; Jahnke, A. A.; Stingelin, N.; Seferos, D. S.; Kim, J.-S. Effects of Side-Chain Length and Shape on Polytellurophene Molecular Order and Blend Morphology. *J. Phys. Chem. C* **2017**, *121*, 2088−2098.
(55) Baldo, M. A.; O'Brien, D. F.; Thompson, M. E.; Forrest, S. R. Excitonic Singlet-Triplet Ratio in a Semiconducting Organic Thin Film. *Phys. Rev. B: Condens. Matter Mater. Phys.* **1999**, *60*, 14422−14428.
(56) Tabachnyk, M.; Ehrler, B.; Gélinas, S.; Böhm, M. L.; Walker, B. J.; Musselman, K. P.; Greenham, N. C.; Friend, R. H.; Rao, A. Resonant Energy Transfer of Triplet Excitons from Pentacene to PbSe Nanocrystals. *Nat. Mater.* **2014**, *13*, 1033−1038.
(57) Zhang, D.; Duan, L.; Li, C.; Li, Y.; Li, H.; Zhang, D.; Qiu, Y. High-Efficiency Fluorescent Organic Light-Emitting Devices Using Sensitizing Hosts with a Small Singlet-Triplet Exchange Energy. *Adv. Mater.* **2014**, *26*, 5050−5055.
(58) Rao, A.; Chow, P. C. Y.; Gélinas, S.; Schlenker, C. W.; Li, C.-Z.; Yip, H.-L.; Jen, A. K.-Y.; Ginger, D. S.; Friend, R. H. The Role of Spin in the Kinetic Control of Recombination in Organic Photovoltaics. *Nature* **2013**, *500*, 435−439.
(59) Chow, P. C. Y.; Gélinas, S.; Rao, A.; Friend, R. H. Quantitative Bimolecular Recombination in Organic Photovoltaics through Triplet Exciton Formation. *J. Am. Chem. Soc.* **2014**, *136*, 3424−3429.
(60) Sulas, D. B.; Rabe, E. J.; Schlenker, C. W. Kinetic Competition between Charge Separation and Triplet Formation in Small-Molecule Photovoltaic Blends. *J. Phys. Chem. C* **2017**, *121*, 26667−26676.
(61) Tsoi, W. C.; Spencer, S. J.; Yang, L.; Ballantyne, A. M.; Nicholson, P. G.; Turnbull, A.; Shard, A. G.; Murphy, C. E.; Bradley, D. D. C.; Nelson, J.; Kim, J.-S. Effect of Crystallization on the Electronic Energy Levels and Thin Film Morphology of P3HT:PCBM Blends. *Macromolecules* **2011**, *44*, 2944−2952.
(62) Burkhart, B.; Khlyabich, P. P.; Thompson, B. C. Influence of the Ethylhexyl Side-Chain Content on the Open-Circuit Voltage in Rr-Poly(3-Hexylthiophene- Co −3-(2-Ethylhexyl)thiophene) Copolymers. *Macromolecules* **2012**, *45*, 3740−3748.
(63) Hoppe, H.; Sariciftci, N. S. Morphology of Polymer/fullerene Bulk Heterojunction Solar Cells. *J. Mater. Chem.* **2006**, *16*, 45−61.
(64) Li, G.; Shrotriya, V.; Yao, Y.; Huang, J.; Yang, Y. Manipulating Regioregular poly(3-Hexylthiophene) : [6,6]-Phenyl-C61-Butyric Acid Methyl Ester Blends—route towards High Efficiency Polymer Solar Cells. *J. Mater. Chem.* **2007**, *17*, 3126.
(65) Collins, B. A.; Gann, E.; Guignard, L.; He, X.; McNeill, C. R.; Ade, H. Molecular Miscibility of Polymer−Fullerene Blends. *J. Phys. Chem. Lett.* **2010**, *1*, 3160−3166.
(66) Westacott, P.; Tumbleston, J. R.; Shoaee, S.; Fearn, S.; Bannock, J. H.; Gilchrist, J. B.; Heutz, S.; DeMello, J.; Heeney, M.; Ade, H.; Durrant, J.; McPhail, D. S.; Stingelin, N. On the Role of Intermixed Phases in Organic Photovoltaic Blends. *Energy Environ. Sci.* **2013**, *6*, 2756.
(67) Kesava, S. V.; Fei, Z.; Rimshaw, A. D.; Wang, C.; Hexemer, A.; Asbury, J. B.; Heeney, M.; Gomez, E. D. Domain Compositions and Fullerene Aggregation Govern Charge Photogeneration in Polymer/Fullerene Solar Cells. *Adv. Energy Mater.* **2014**, *4*, 1400116.
(68) Jamieson, F. C.; Domingo, E. B.; McCarthy-Ward, T.; Heeney, M.; Stingelin, N.; Durrant, J. R. Fullerenecrystallisation as a Key Driver of Charge Separation in Polymer/fullerene Bulk Heterojunction Solar Cells. *Chem. Sci.* **2012**, *3*, 485−492.

DOI: 10.1021/acsaem.8b01023
ACS Appl. Energy Mater. 2018, 1, 5033−5042